Synoptic moisture pathways associated with mean and extreme precipitation over Canada for winter and spring

Xuezhi Tan[1,2] · Thian Yew Gan[2] · Yongqin David Chen[3]

Abstract

Dominant synoptic moisture pathway patterns of vertically integrated water vapor transport (IVT) in winter and spring over Canada West and East were identified using the self-organizing map method. Large-scale meteorological patterns (LSMPs), together with synoptic moisture pathway patterns, were related to the variability in seasonal precipitation totals and occurrences of extreme precipitation events. Changes in both occurrences of LSMPs and seasonal precipitation occurred under those LSMPs were analyzed to explain observed changes in seasonal precipitation totals and occurrences of extreme precipitation events. The effects of large-scale climate anomalies on occurrences of LSMPs were also examined by composite analyses. Results show that synoptic moisture pathways and LSMPs exhibit the propagation of jet streams resulting from the Rossby wave resonance, as the location and direction of ridges and troughs, and the strength and center of pressure lows and highs varied considerably. Even though LSMPs resulting in positive precipitation anomalies are associated with more frequent occurrences of extreme precipitation events than those resulting in negative precipitation anomalies, the patterns featured with anomalously low IVT are sometimes associated with more frequent occurrences of extreme precipitation events. Significant decreases in occurrences of synoptic moisture pathway patterns that are favorable with positive precipitation anomalies and more precipitation extremes in winter over Canada West, and significant decreases in seasonal precipitation and occurrences of precipitation extremes under most synoptic moisture patterns resulted in decreases in seasonal precipitation and the occurrence of extreme precipitation events. LSMPs resulting in a hot and dry (cold and wet) climate and less (more) frequent extreme precipitation events over the Canadian Prairies in winter and northwestern Canada in spring are more likely to occur in years with a negative (positive) phase of PNA. Occurrences of LSMPs for a wet climate and frequent occurrences of extreme precipitation events over southeastern Canada are associated with a positive phase of NAO. In El Niño years or negative PDO years, occurrences of LSMPs tend to associate with a dry climate and less frequent precipitation extremes over western Canada.

Keywords Vertically integrated water vapor transport · Synoptic patterns · Large-scale meteorological patterns · Seasonal precipitation · Extreme precipitation · Self-organizing maps, climate anomalies

✉ Xuezhi Tan
  tanxuezhi@mail.sysu.edu.cn

1   Department of Water Resources and Environment, School of Civil Engineering, Sun Yat-sen University, Guangzhou 510275, People's Republic of China

2   Department of Civil and Environmental Engineering, University of Alberta, Edmonton, AB T6G 2W2, Canada

3   Department of Geography and Resource Management, Institute of Environment, Energy and Sustainability, The Chinese University of Hong Kong, Hong Kong, People's Republic of China

1 Introduction

The northern high-latitude regions have experienced the most rapid warming compared with mid- and low-latitudes over the past half century (IPCC 2013; Najafi et al. 2015). The warming rate of annual mean temperature over the high-latitude regions was almost twice that of the global average (Walsh 2014), commonly referred to as Arctic amplification (Cohen et al. 2012; Screen and Simmonds 2010). Canada has a vast high-latitude landmass that has been experiencing rapid warming by a nationwide average warming of 1.5 °C in annual mean surface air temperature over 1950–2010 (Vincent et al. 2015). The warming was accompanied by both

positive and negative changes in annual precipitation totals and extremes in different part of Canada (Mekis and Vincent 2011; Vincent et al. 2015), albeit pan-Arctic precipitation is consistently projected to increase over the twenty-first century by climate models as a by-product of Arctic amplification (Bintanja and Selten 2014; Barry and Gan 2011).

A warmer climate has resulted in an intensified hydrologic cycle of northern Canada (Déry et al. 2009) and an increased poleward moisture transport to the Eurasian Arctic river basins (Zhang et al. 2013), even though no significant changes in meridional moisture transport over Northern Canada were found in reanalyses data (Dufour et al. 2016). The intensified water cycle may have some implications to the magnitude, frequency, and severity of extreme weather phenomena, such as droughts, intensive storms, and floods that are costliest natural disasters for Canada (White and Etkin 1997). However, the physical mechanisms behind changes in water-related regional climate extremes are complicated, since both thermodynamic and dynamic changes, and their interactions could result in changes in precipitation extremes (Collins et al. 2018; Wang et al. 2017; Zhang et al. 2017).

Changes in precipitation during the cold seasons over Canada have widespread impacts on regional water resources availability, the ecosystem, agriculture, forestry, and economic activities (Barnett et al. 2005). For southern Canada, snowmelt streamflow and rainfall-induced runoff are important water sources for municipal water supply, hydropower production, and agricultural production (Schindler and Donahue 2006; Gan 2000). Snowpack is of great significance to ski recreation (Gilaberte-Búrdalo et al. 2014). For northern Canada, because warming is proceeding more rapidly, and precipitation is projected to increase more substantially (Bintanja and Selten 2014) and to shift from snow-dominated to rain-dominated precipitation (Bintanja and Andry 2017), northern ecosystems are particularly sensitive to warming and precipitation changes. Therefore, it is beneficial to understand the variability and change in seasonal precipitation totals and extremes that have profound implications for Canada dominated by snow.

The interannual and interdecadal variability of precipitation are largely modulated by the coupling of large-scale atmospheric circulations (Newton et al. 2014) and water vapor transport (Skific et al. 2009). Precipitation processes are driven by the mid-tropospheric circulation that forces vertical motions of the atmosphere and the advection of cold and warm fronts at the surface (Holton 2004). Winter cyclonic activities have become significantly more frequent, durable, and stronger in southern Arctic of Canada, but weaker and less frequent in southern Canada, especially along southwestern coasts (Wang et al. 2006). Newton et al. (2014) linked winter temperature, precipitation totals, and droughts across Canada to synoptic circulation patterns.

However, how circulation patterns are associated with moisture pathway patterns have not been examined to explore physical mechanisms behind occurrences of extreme precipitation events in Canada. Effects of changes in atmospheric circulation on seasonal precipitation totals and extremes of Canada are also needed to be examined, especially under effects of Arctic amplification (Vavrus et al. 2017).

The objective of this study is to evaluate seasonal precipitation totals and extremes over Canada using a SOM-based clustering method. We first identified synoptic conditions of large-scale meteorological patterns (LSMPs) that control the magnitude and occurrences of precipitation. Then, we linked changes in occurrences of LSMPs to changes in seasonal precipitation and occurrences of precipitation extremes. In a companion study, Tan et al. (2018b) investigated characteristics of LSMPs conducive to seasonal precipitation totals and occurrences of precipitation extremes of Canada in warm seasons (i.e., summer and fall). This paper addresses LSMPs associated with seasonal precipitation totals and occurrences of precipitation extremes of Canada in cold seasons (i.e., winter and spring). These efforts will improve our understanding of the spatial and seasonal variability of precipitation and occurrences of precipitation extremes that are possibly caused by the variability and changes in moisture pathways and large-scale atmospheric circulations.

This paper is organized as follows: In Sect. 2 we briefly describe observed precipitation data and large-scale meteorological data obtained from atmospheric reanalysis including vertically integrated water vapor transport (IVT), geopotential height, and temperature. In Sect. 3, we describe the method of self-organizing mapping (SOM) and methods used to relate seasonal precipitation totals and extremes to moisture pathway patterns and atmospheric circulations. Results are presented in Sect. 3. Summary and conclusions are presented in Sect. 4.

2 Data and methods

2.1 JRA-55 IVT reanalysis and Canadian ANUSPLIN precipitation data

To create a catalog of dominant LSMPs, we analyzed the gridded ($0.5625° \times 0.5616°$) daily IVT, surface mean daily temperature, and 500 hPa geopotential height (GPH) fields of 1958–2013, taken from the Japanese 55-year Reanalysis (JRA-55) (Kobayashi et al. 2015) dataset using the self-organizing maps (SOMs) method. The JRA-55 dataset is the second Japanese global atmospheric reanalysis dataset which is a comprehensive dataset suitable for studying multi-decadal variability and climate change. The JRA-55 IVT data were widely used for water cycle analyses for northern high-latitude regions including Arctic regions (e.g., Bintanja and

Andry 2017; Hu et al. 2016; Vihma et al. 2015) and Canada (Kochtubajda et al. 2017) because of its good performance in representing water cycle and water balance of northern high-latitude regions (Harada et al. 2016) and relatively long data set beginning in 1958. For this study, we analyzed the atmospheric fields for cold seasons, i.e., winter (December–February) and spring (March–May).

To relate seasonal precipitation totals and occurrences of extreme precipitation events to LSMPs, high-resolution (~ 10 km) gridded daily Canadian precipitation data (1958–2013) recently developed by Hutchinson et al. (2009) using the Australian National University Spline (ANUSP-LIN) interpolation scheme, were used to identify seasonal precipitation totals and days with extreme precipitation at each grid box over Canada West and East. The ANUSPLIN dataset that covers the landmass of Canada was derived from observed precipitation data of nearly 3000 stations of Environment Canada. Even though there are some minor discrepancies between station extreme precipitation and ANUSP-LIN extreme precipitation (Benyahya et al. 2014; Hopkinson et al. 2011), the ANUSPLIN dataset provides country-wide, high-resolution daily precipitation data for historical climate analysis. Until now, the ANUSPLIN dataset is likely the best published station-based, gridded daily precipitation dataset that has been widely used to study historical climate of Canada (e.g., Benyahya et al. 2014; Cannon et al. 2015; Gizaw and Gan 2016; Newton et al. 2014; Radić et al. 2015). To validate the gridded ANUSPLIN precipitation data for analyzing extreme precipitation in this study, we have also analyzed 164 (131) stations of daily precipitation data of Canada West (East) over 1958–2005 obtained from Mekis and Vincent (2011) which were incorporated into the ANUSPLIN precipitation dataset, with the same method adopted in this study. The station analysis results for regions with dense stations are consistent to those obtained from the ANUSPLIN precipitation dataset. Therefore, we only we present the analysis results based on the ANUSPLIN precipitation dataset.

2.2 Large-scale meteorological patterns (LSMPs) identified by the SOMs method

The SOMs method (Kohonen 1998) is a relatively new approach to cluster synoptic climatology, and diverse applications of SOMs have been increasing (Sheridan and Lee 2011). Because SOMs are capable of reducing the dimensionality of climate data to a representative size for spatial pattern analysis, extreme weather or climate events could be linked to representative circulation patterns. Thus, changes in climate extremes could be attributed to changes in representative circulation patterns identified from the application of SOMs for studying climate extremes. SOMs have been widely used to display and to analyze the characteristic behavior of atmospheric and oceanic circulation patterns, as well as to link regional climate variables (i.e., temperature and precipitation) to these patterns (Cassano et al. 2015, 2016; Gibson et al. 2017; Horton et al. 2015; Lennard and Hegerl 2015; Loikith et al. 2015). SOMs, a type of neural network algorithm, use an unsupervised learning approach to cluster input data into limited representative groups (patterns). The neighboring output patterns are generally more similar than distant output patterns. Because SOMs, being a nonlinear clustering method, can isolate nonlinear patterns, SOMs have advantages over linear methods such as empirical orthogonal function analysis that could be problematic for highly nonlinear systems (Reusch et al. 2005). Given geoscience data are ever growing with higher spatial and temporal resolutions, and becoming more complex, SOMs have been useful to reduce the dimensionality and the organization of large geoscience data set. Swales et al. (2016) has hierarchically trained SOMs on the magnitude of the standardized IVT anomaly (|IVT|′) to identify different moisture delivery mechanisms for extreme rainfall in the US Mattingly et al. (2016) has applied SOMs to IVT data with the seasonal cycle removed to link the trends of mass loss of Greenland ice sheet with increases of moisture transport to Greenland.

In this study, we applied SOMs to cluster the |IVT|′ to examine different moisture pathway patterns associated with seasonal precipitation totals and extremes across Canada. The anomaly of the magnitude of IVT were computed by subtracting the monthly means from the total field and were then normalized by dividing the anomaly values by the standard deviation of the local daily data in that month over all years to obtain the |IVT|′. For every season and region, the SOM was first trained on the |IVT|′ to examine synoptic moisture pathways. The regional domains for |IVT|′ extend from 180°W to 100°W and 40°N to 80°N for Canada West, and 100°W to 25°W and 40°N to 80°N for Canada East, respectively, which include both land and marine areas (Fig. 1). Since we aimed to identify the variability of synoptic moisture transport over both land and ocean regions, we trained the land and ocean |IVT|′ together, instead of highlighting IVT anomalies over land to cluster synoptic moisture transport that were done in Swales et al. (2016) and Alexander et al. (2015).

We tested four SOM configurations: a 4-node SOM (2 columns × 2 rows), a 9-node SOM (3 columns × 3 rows), a 12-node SOM (4 columns × 3 rows), and a 16-node SOM (4 columns × 4 rows) applied to |IVT|′ data. For each test, SOM nodes were explored using a variety of SOM node configurations and parameters, such as neighborhood function, learning rate, and radius. Results show that dominant patterns were not sensitive to the SOM configuration and parameters. From results of these tests, we eventually chose the 9-node |IVT|′ SOM as the best clustering for
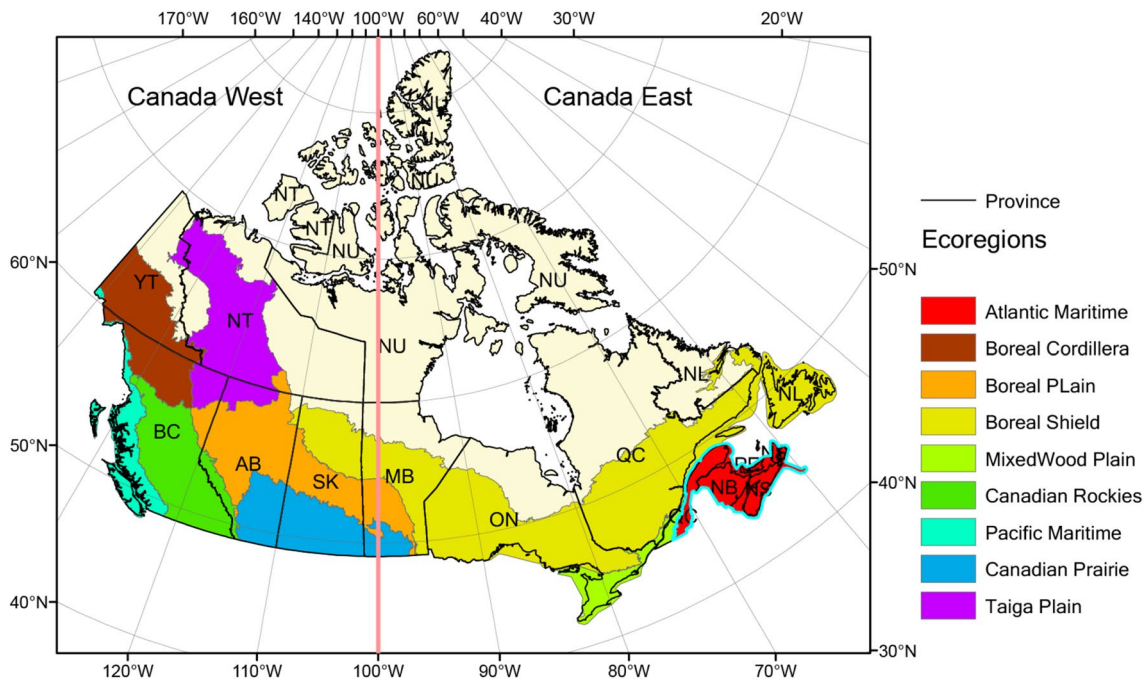
Fig. 1 Provinces and ecoregions of Canada. The red vertical line divides Canada into Canada West and East analyzed in this study. The Provinces or Territories of Canada are: *AB* Alberta, *SK* Saskatchewan, *MB* Manitoba, *NL* Newfoundland and Labrador, *PE* Prince Edward Island, *NS* Nova Scotia, *NT* Northwest Territories, *NU* Nunavut, *ON* Ontario, *NB* New Brunswick, *YT* Yukon Territory, British Columbia, *QC*, Quebec

analyzing precipitation of Canada. Each SOM node represents a |IVT|′ pattern. The nine-output |IVT|′ patterns derived from the 9-node SOM is sufficient to show some infrequently occurred |IVT|′ anomalies and to represent the continuum of moisture pathway patterns without involving excessive intra-node variability. The nine output |IVT|′ patterns are also easier to interpret than those derived from the 16-node SOM.

Once the 3×3 SOM array for |IVT|′ has been created, the |IVT|′ data were 'mapped', in which each daily |IVT|′ was compared with each |IVT|′ pattern to identify the pattern to which a daily |IVT|′ best matches. Thus, each daily |IVT|′ was classified to one of the nine |IVT|′ patterns. This mapping procedure generated a list of node number corresponding to each daily |IVT|′, which allows us to determine the occurrence frequency of each |IVT|′ pattern. For each |IVT|′ pattern, the composite averages of GPH, surface temperature, and IVT vector fields were also computed by relating each daily field to that |IVT|′ pattern occurring on that day. To more clearly identify the atmospheric circulations and maximally capture an entire low or high-pressure system that links to each |IVT|′ pattern, the regional domain of these composites was expanded to the whole country. In this study, |IVT|′ patterns and composites of GPH, surface temperature, and IVT vector are together referred to as LSMPs.

2.3 Mapping mean and extreme precipitation

We defined extreme precipitation events as the top 5% and 1% of days of daily precipitation larger than 0.2 mm that occurred in each season during the 56-year period. This definition of precipitation extremes results in about 6.0 (top 5%) and 2.0 days (top 1%) of extreme precipitation events per season in a year, which ensures sufficient samples for this study. For seasonal precipitation totals, the daily precipitation at each grid box on each day was related to the |IVT|′ pattern occurring on that day. Daily precipitation anomaly corresponding to a |IVT|′ pattern was derived by subtracting the mean daily precipitation for that |IVT|′ pattern from the overall mean daily precipitation for all days of each season. For extreme precipitation events, a day with extreme precipitation was related to a |IVT|′ pattern that occurred on that day. For each grid box, the frequency of extreme precipitation events that have occurred on a |IVT|′ pattern was the ratio of the total number of extreme precipitation events for that |IVT|′ pattern to that for all the nine |IVT|′ patterns. These analyses produced maps relating each |IVT|′ pattern to seasonal precipitation anomalies and the occurrence frequency of extreme precipitation events across Canada. By so doing, we can identify LSMPs that are responsible for seasonal precipitation and extreme precipitation events.

2.4 Changes in occurrences of LSMPs and precipitation

Transition frequencies from one pattern to other pattern could show how LSMPs are temporally related to each other (Mieruch et al. 2010; Swales et al. 2016). Because |IVT|′ patterns and composites (LSMPs) result from |IVT|′ and GPH, surface temperature, and IVT vector fields of individual days, we further examined all days involved in each |IVT|′ pattern and trends of each LSMP occurred in each year for each season during 1958–2013. Here we calculated following characteristics of LSMPs: (1) the total number of days on which each |IVT|′ pattern had occurred (occurrence, day year^{-1}); (2) the mean length of consecutive occurrences of each |IVT|′ pattern (persistence, day event^{-1}); and (3) the longest consecutive occurrence (maximum duration, day event^{-1}); (4) the 1-day lead transition frequency for all nine |IVT|′ patterns (transition matrix, %). For the former three characteristics, a trend analysis over 1958–2013 was conducted by the nonparametric Mann–Kendall (MK) test (Kendall 1975) at the 0.05 significance level. The trends of seasonal precipitation totals and the extreme precipitation events occurred in each |IVT|′ pattern were also tested by the MK test. The magnitude of changes in these characteristics was estimated by the Theil–Sen estimator (Sen 1968).

2.5 Teleconnections between LSMPs and large-scale climate anomalies

Some interannual and interdecadal variabilities in dominant atmospheric circulations and hydroclimatic variables over Canada are related to large-scale teleconnections (Coulibaly 2006; Gan et al. 2007; Newton et al. 2014; Tan et al. 2016), such as Pacific North American (PNA) pattern, El Niño-Southern Oscillation (ENSO), Pacific Decadal Oscillation (PDO), North Atlantic Oscillation (NAO) and Arctic Oscillation (AO). We used climate indices that represent the above five climate oscillations to evaluate the teleconnection between occurrences of LSMPs and precipitation for each season over Canada West and East. The multivariate ENSO index (MEI) (Wolter and Timlin 2011) was used to represent ENSO. The cold (warm) ENSO phase, i.e., La Niña (El Niño), is represented by negative (positive) values of the MEI. Daily values of the MEI, PNA, PDO, NAO, and AO indices were obtained from the Climate Prediction Centre (http://www.cpc.ncep.noaa.gov/).

Each daily teleconnection distribution was divided into three conditions, i.e., positive, neutral, and negative conditions of the 56 years included in the study period. This procedure was widely used to categorize teleconnections (e.g., Bonsal et al. 2001; Newton et al. 2014). We linked MEI, PDO, PNA, NAO and AO conditions to each |IVT|′ anomaly pattern as composite teleconnection conditions, on daily, monthly and seasonal scales. To show the possible lag effects of teleconnection on LSMPs, we calculated the 0-, 1-, 2-, and 3-month lag time composites of teleconnection conditions for each |IVT|′ pattern. We used the two-sample nonparametric Kolmogorov–Smirnov test to evaluate the differences in synoptic type frequency distributions for each positive–negative pair at the 0.05 significance level.

3 Results

3.1 Changes in precipitation totals and occurrence of extreme precipitation events

Figure 2 shows changes in precipitation totals and occurrences of extreme precipitation events in winter and spring derived from the ANUSPLIN precipitation dataset. Changes in seasonal total precipitation in both winter and spring are statistically significant over entire Canada as detected by the MK test. Winter precipitation has mainly increased in northern Canada but decreased in southern and central Canada during 1958–2013, although some areas in southern Ontario, southern British Columbia have also experienced significant increasing trends (Fig. 2a). However, spring precipitation increased in southern and northern Canada but decreased in Yukon Territory, southern Northwest Territories, and northern Canadian Prairie provinces (Fig. 2b). The seasonal precipitation totals averaged over the west (east) indicate a significant decrease (increase) of −21.5 (25.9) mm in winter, while spring precipitation over the west and east increased by 39.0 and 77.1 mm, respectively, during the past 56 year.

Similar to trends of seasonal precipitation totals, the occurrence of heavy (5%) precipitation and extreme (1%) precipitation events also showed an overall decrease in winter and a marginal increase in spring (Fig. 2c), while a statistically significant increase in northern Canada in both winter and spring (Fig. 2d). Statistically significant changes in the occurrence of heavy and extreme precipitation identified by Poisson regression were denoted with blue contours in Fig. 2c–f. As expected, there are more spatial variabilities in occurrences of extreme precipitation events than those of precipitation totals. The occurrence frequency of heavy precipitation events is much more significant and more spatially consistent than that of extreme precipitation events (Fig. 2c–f). Therefore, we only further report results of heavy precipitation as an indicator of the extreme precipitation, unless otherwise specified. Because both Canada West and East have experienced a mix of increasing and decreasing trends in extreme precipitation, the overall areal-weighted average of decrease (increase) in occurrences of extreme precipitation is −0.025 (0.156) events per year over Canada West in winter (spring), and Canada East has experienced an increase of 0.167 and 0.245 events per year in

Fig. 2 Changes in the mean seasonal precipitation (**a, b**), occurrence of heavy precipitation events defined with days when precipitation exceed 95% of daily precipitation of wet days in a season (**c, d**), and occurrence of extreme precipitation events defined with days when precipitation exceed 99% of daily precipitation of wet days in a season (**e, f**). Grid cells with statistically significant trends in the occurrence of heavy and extreme precipitation identified by Poisson regression were within blue contours. All grid cells are with statistically significant trends in seasonal precipitation totals. The left column (**a, c, e**) shows trends for the winter season while the right column (**b, d, f**) shows trends for the spring season
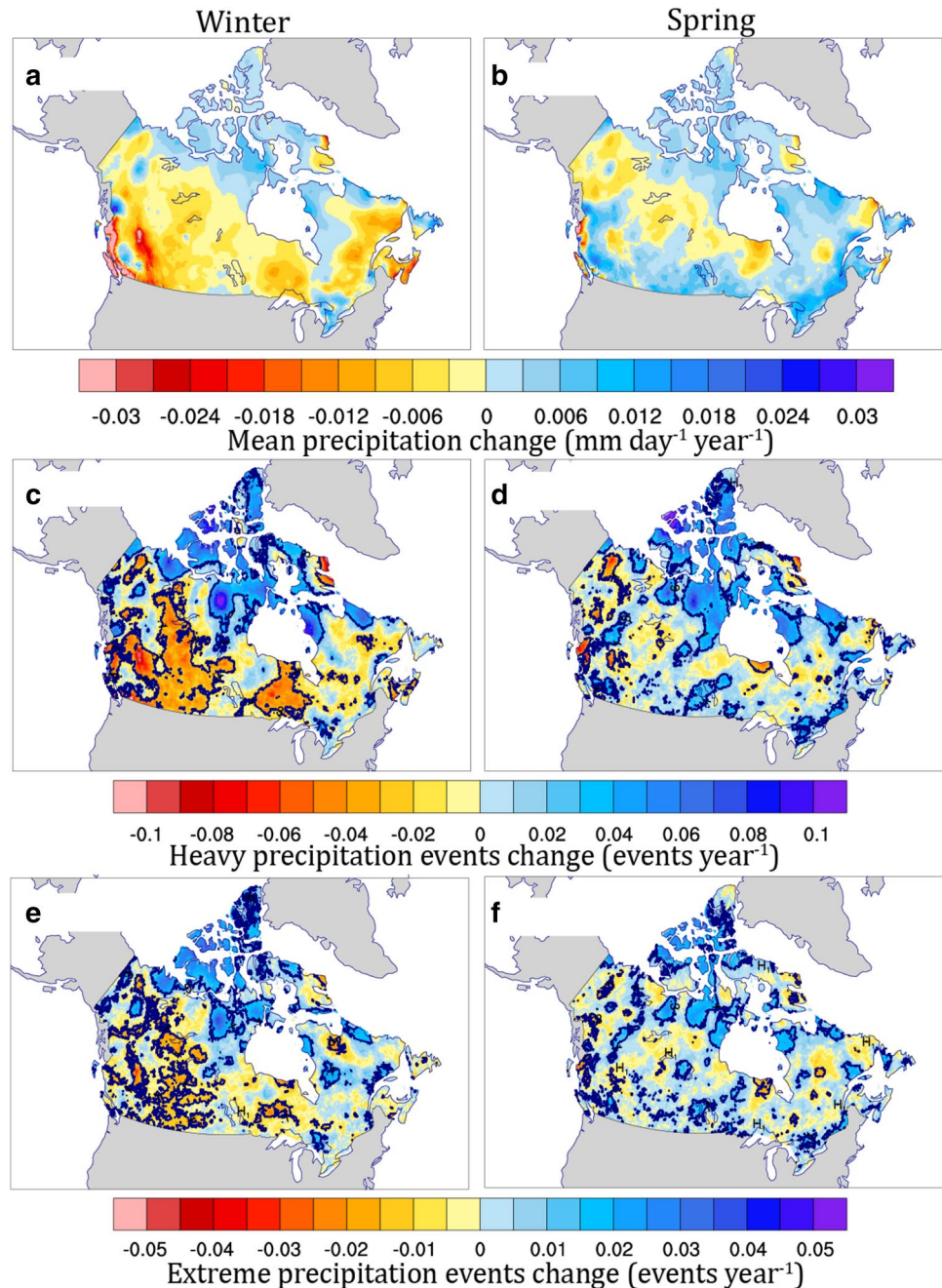
winter and spring, respectively, during the past 56 year. Note that the average number of all seasonal extreme precipitation is about 2 events per year.

3.2 LSMPs features

Daily |IVT|′ was classified into nine patterns (nodes) on a 3×3 SOM array (Fig. S1 for winter and Fig. S2 for spring, respectively) for Canada West (Figs. S1a and S2a) and East (Figs. 3b, 4b). Nine synoptic |IVT|′ patterns exhibit varying centers of extremely high and low |IVT|′ from Node S1 to S9

for both regions and both seasons. Neighboring nodes show the strongest similarities while the largest variance of the spatial distribution of |IVT|′ is shown in nodes with the largest separation, particularly for nodes in opposing corners. Different spatial distributions of |IVT|′ result from different pathways for transporting moisture to different regions, which can be identified by integrated interpretation of |IVT|′ patterns and circulation patterns (Figs. S3, S4). To more generally describe LSMPs and moisture pathway patterns, we grouped some similar |IVT|′ nodes for each season and each region, based on the central locations and their evolution of

extremely large |IVT|′ values (dark blue regions in Figs. S1, S2). Each node was assigned to one of four pattern clusters which are the dry, north, west and central pattern clusters for Canada West, and the dry north, south and east pattern clusters for Canada East, respectively. The latter three pattern clusters are wet |IVT|′ patterns showing anomalous high |IVT|′ over particular regions, while the dry pattern cluster exhibits a nationwide anomalous low |IVT|′. As expected, for both regions and both seasons, the regions with extremely high |IVT|′ are located around the ridge for each node, and the magnitude of the extremely large |IVT|′ on each node is associated with the strength of high-pressure ridge shown on that node. The dry pattern generally corresponds to a typical circulation without an evident high-pressure ridge over the study region.

To avoid presenting too many details, we only show four |IVT|′ patterns and their associated seasonal precipitation totals and occurrences of precipitation extremes in the main text, while all the 9 patterns are presented in Supplementary Figures. In the 9 patterns, the selected four patterns (the first row of Figs. 3, 4, 5, 6) represents four pattern clusters that are primarily associated with spatiotemporal variabilities of regional precipitation. The corresponding composites of 500-hPa GPH, surface temperature anomalies, and IVT fields for the nine |IVT|′ patterns were shown in the second row of Figs. 3, 4, 5 and 6 for winter and spring, respectively. The composite maps show comprehensive climatological features of LSMPs identified from a variety of spatial clusters of surface temperature anomalies, IVT vectors, pressure highs and lows, and ridges and troughs over North America, North Pacific, North Atlantic and Arctic. For atmospheric systems where the trough points south and the ridge points north, regions of mid-tropospheric convergence (divergence), located to the right (left) of a ridge axis and left (right) of a trough, are concurrent with surface divergence (convergence), consequently suppressing (facilitating) cloud formation and precipitation. Therefore, mid-tropospheric ridges and troughs generally determine the location of regions where precipitation events occur. For the region that is located in the east of the Rocky Mountains, lee cyclogenesis is of great importance for efficiently generating precipitation (Lackmann and Gyakum 1996; Spence and Rausch 2005).

For LSMPs over Canada West in winter, the North (Fig. 3e) and West pattern (Fig. 3g) clusters exhibit a high-pressure system with the center shifted southeast from the Gulf of Alaska to southwestern Canada which shows the movement of pathways for transporting moisture to Canada West. A strong ridge over the Pacific Ocean in Nodes S1-S2 results in northerly meridional flow directing cold Arctic air over the south of Canada West, while an Aleutian Low and Gulf cyclone across Canada West and Alaska in Nodes S3 (Fig. 3e) forces moisture from North Pacific to the north of

Canada West. Nodes S3–S5 also show various ridges over western North America with different strengths and positions which block the flow of cold Arctic air into the south of Canada West (Bonsal et al. 2001; Newton et al. 2014; Rutz et al. 2015). Nodes S1–S5 indicates a significantly wavy mid- and high-latitude atmospheric circulation over North America (Fig. S3a) for moisture pathways that could associate with jet streams resulting from the anticyclonic or cyclonic nature of the Rossby wave breaking event (Liu and Barnes 2015). The dry pattern depicts more zonal flow (Fig. 3d) and a split-flow blocking high (Fig. S3a), resulting in anomalously high temperature over Canada West.

Past studies have examined some moisture pathways that can lead to mild or extreme precipitation events for some particular regions of Canada. Brimelow and Reuter (2005) found that the Gulf of Mexico can be moisture sources for precipitation in southern Canada when the Great Plains low-level jet stream (storm track) to Dakotas is concurrent with cyclogenesis centered over the Canadian Prairies. Negative anomalies of precipitation over central and western Canadian Prairies were linked with low moisture transport from the Pacific Ocean (Gulf of Mexico) in the winter (summer) (Liu et al. 2004). Both the Arctic and Pacific Oceans are moisture sources of winter precipitation for the Saskatchewan River Basin in the Canadian Prairies (Liu and Stewart 2003). The transport of moisture for the Mackenzie River Basin with 1.8 million km^2 in basin area, has high spatiotemporal variabilities (Smirnov and Moore 1999, 2001). Specifically, during autumn, winter, and spring, extratropical cyclones transport moisture from the subtropical and mid-latitude central Pacific Ocean into the Mackenzie River Basin, while moisture from the Arctic Ocean enters the Mackenzie River Basin during the summer. Characterized by a relatively elongated band of concentrated moisture and strong, low-level wind in the atmosphere (Dettinger 2011; Tan et al. 2018a), atmospheric river events in mid-latitude Pacific Ocean trigger extreme precipitation events in British Columbia (Roberge et al. 2009; Spry et al. 2014; Tan et al. 2018a).

The waviness of circulation in spring for Canada West is less evident than that in winter (Fig. 4e–h), even though the Aleutian Low and Gulf cyclone across Canada West and Alaska are evident in some nodes (Fig. 4f). The North pattern cluster (Fig. 4e) exhibits strong ridges over western Canada and the ridge shifts eastward from British Columbia to Canadian Prairie Provinces. The West pattern cluster (Fig. 4f) shows a weak trough over western Canada, while the dry pattern (Fig. 4h) shows significant zonal flow. However, the Central pattern cluster (Fig. 4g) indicates both troughs over the North Pacific and ridges over western Canada.

For LSMPs over Canada East in winter (Fig. 5e–h), nine nodes generally show troughs stretching from Arctic Canada
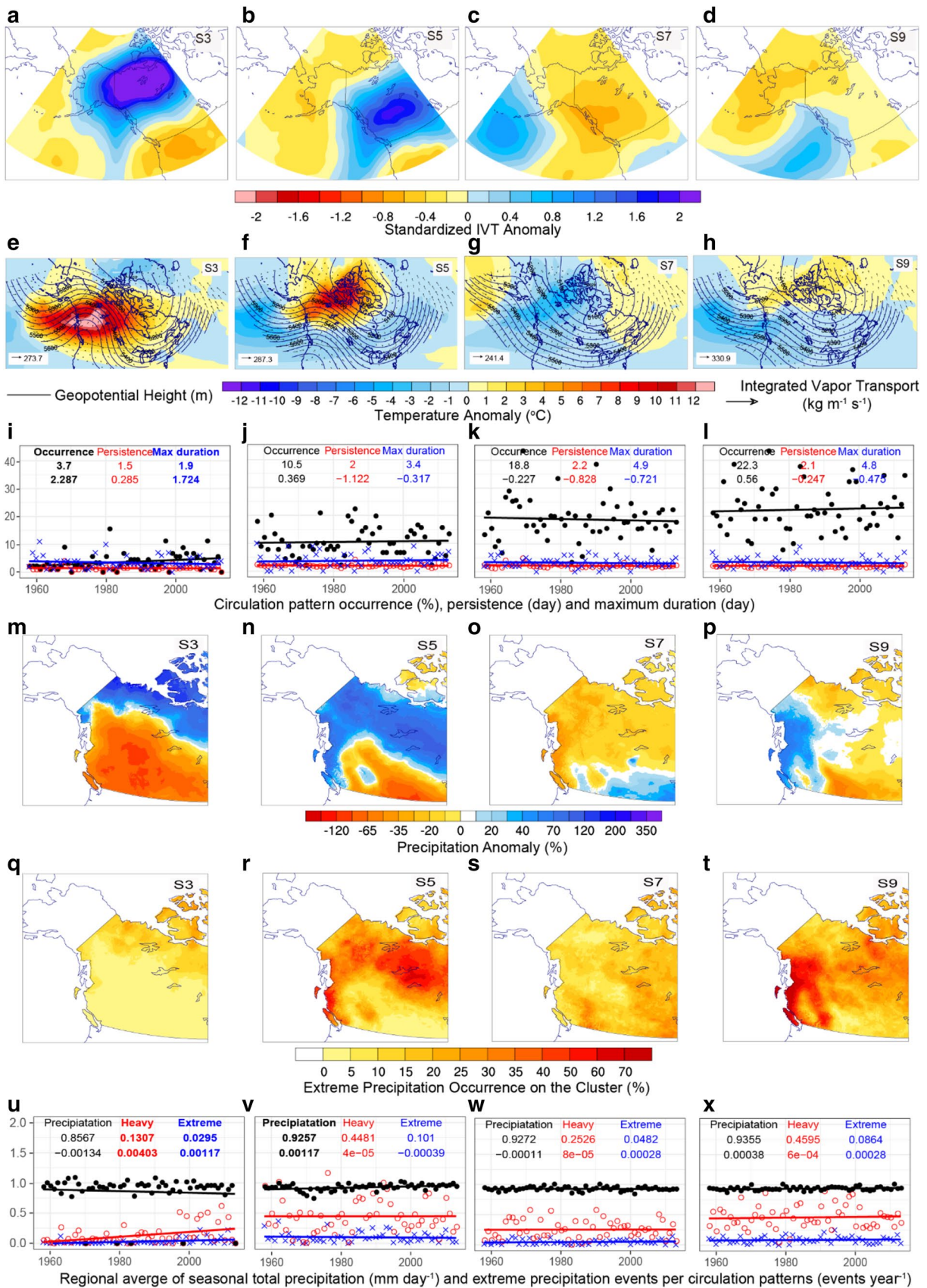
Geopotential Height (m) — Temperature Anomaly (°C) — Integrated Vapor Transport (kg m⁻¹ s⁻¹)

Standardized IVT Anomaly

Circulation pattern occurrence (%), persistence (day) and maximum duration (day)

Precipitation Anomaly (%)

Extreme Precipitation Occurrence on the Cluster (%)

Regional averge of seasonal total precipitation (mm day⁻¹) and extreme precipitation events per circulation patterns (events year⁻¹)

◀**Fig. 3** Spatiotemporal variability of moisture transport patterns and their associated seasonal precipitation totals and extremes in *winter* over *Canada West*. **a–d** Four SOM nodes of standardized integrated vapor transport anomaly (|IVT|′) were selected from the 3×3 SOM nodes showing in Supplementary figures. **e–h** Composite large-scale atmospheric circulation patterns shown by geopotential heights in contours, IVT fields in vectors and surface temperature anomalies in shaded colors. **i–l** Time series of SOM |IVT|′ pattern occurrences (occurrences; %) in black, the mean length of consecutive occurrence (persistence; days event^{-1}) in red, and maximum duration (max duration; days event^{-1}) in blue. **m–p** Four patterns of daily precipitation anomalies derived form high-resolution ANUSPLIN precipitation dataset mapped onto SOM |IVT|′ patterns shown in **a–d**. Daily precipitation anomalies were calculated as the percentage of mean daily precipitation occurred in days with a SOM |IVT|′ pattern in each grid cell relative to the 1958–2013 mean daily precipitation at each grid cell in all days. **q–t** Probability of heavy precipitation occurred in each SOM |IVT|′ patterns shown in a-d derived from high-resolution ANUSPLIN precipitation dataset. **u–x** Time series of the area-weighted mean of seasonal average daily precipitation (black; mm day^{-1}), number of heavy (red) and extreme (blue) precipitation events (days) per pattern occurrence, referred to throughout the text as a measure of the seasonal precipitation totals and occurrence frequency of precipitation extremes associated with each pattern. In **i–l** and **u–x**, the corresponding mean values (the first row of numbers) and the Theil–Sen slope of the trend line (the second row of numbers) in 1958–2013 are also presented. Statistically significant trends (5% significance level) are shown by bold font in the scatter plots. The area-weighted mean daily precipitation and occurrences of extreme precipitation events for all winter days over Canada West are 0.876 mm day^{-1} and 2.2 days (average of 0.245 days for 9 SOM |IVT|′ patterns), respectively

to Canada East with varying directions and strength, even though ridges stretching from particular regions of North Atlantic intrude to Canada East. Specifically, the North pattern cluster (Fig. 5e) exhibits troughs stretching from the Hudson Bay to the Atlantic Maritime concurrent with ridges stretching from the North Atlantic to Arctic Canada. The South pattern cluster (Fig. 5f) only shows troughs over Canada East, while the East pattern cluster (Fig. 5g) also shows troughs that westward shift to Canada East compared to those of the North pattern cluster. The dry pattern (Fig. 5h) shows a typical zonal flow across Canada East. LSMPs over Canada East in spring (Fig. 6e–h) is pairwise similar to those in winter (Fig. 5e–h), except that low-pressure troughs are weaker in spring and high-pressure ridges westward shifts to Canada East, compared to those in winter.

For eastern Canada, synoptic structures that are responsible for precipitation events over different regions were rather disparate both in the warm season (Milrad et al. 2014) and cold season (Milrad et al. 2009a, b). For example, precipitation over the south of Canada East is related to a strong anticyclone downstream of the center of Canada East. Precipitation over the southwest of Canada East is related to a strong cyclone centered over the Gulf of Mexico, and precipitation over the west of Canada East is related to a weak Alberta clipper system that intensifies rapidly before reaching the Atlantic Ocean (Milrad et al. 2010). While moisture

studies had generally been focusing on particular regions of Canada, Tan et al. (2018a) identified some moisture sources and dominated pathways that are associated with precipitation extremes of different seasons and regions across the whole country.

3.3 Changes in occurrence characteristics of LSMPs

We estimated three occurrence characteristics of LSMPs (frequency, persistence and maximum duration) for two seasons and two regions in each year. Thus, we obtained 108 (3×9×2×2) time series of the pattern occurrence characteristics (the third row of Figs. 3, 4, 5, 6). Trend analyses on these time series indicate that 19 (17.6%) occurrence characteristics of LSMPs show statistically significant trends during 1958–2013 (Fig. 7). More spring LSMPs show significant trends in occurrence characteristics (11 out of 54) than winter LSMPs (8 out of 54). More |IVT|′ patterns experienced trends in the occurrence frequency (8 out of 36) than persistence (5 out of 36) and maximum duration (6 out of 36). Canada East (12 out of 54) shows trends that are more significant in occurrence characteristics than Canada West (7 out of 54).

For Canada West in winter, the significant increase in the occurrence of the wet pattern (Fig. 3i) and non-significant increase in the occurrence of Nodes S1, S4, S5, and S9 coincide with the non-significant decrease in the occurrence of anomalously high |IVT|′ over Alaska (Nodes S2 and S4). The increase in the occurrence of Nodes S1, S3, S4 and S5 indicates an increase of IVT to the landmass of Canada West in winter, which agrees on the increase in the poleward moisture transport from the North Pacific to Arctic (Liu and Barnes 2015; Zhang et al. 2013). However, the IVT over the southern landmass of Canada East in winter increased while those of the north decreased, as many patterns showing anomalously high |IVT|′ over southern part of Canada West (Fig. 3b) have replaced patterns showing anomalously high |IVT|′ over Arctic Canada (Fig. 3a).

The occurrence of anomalously high |IVT|′ over northwestern Canada and the Gulf of Alaska had decreased significantly in spring because of decreases in the occurrence frequency, persistence and maximum duration of Node S5 (Fig. 4k). |IVT|′ over the south of Canada West (Node S6) and the west of Arctic Canada (Node S1) shows a significant increase in spring. Similar to changes in |IVT|′ anomaly patterns for Canada East in winter, decreases in the occurrence of dry patterns (Fig. 4l) had led to increases in the occurrence of most nodes included in the North and South pattern clusters (Nodes S1 and S4–S7). Patterns for Canada East (Nodes S2–S3 and S8–S9) showing a decrease in occurrences in spring are associated with a region shifted eastward with anomalously high |IVT|′, compared to patterns (Nodes S1 and S4–S7) showing an increase in occurrences
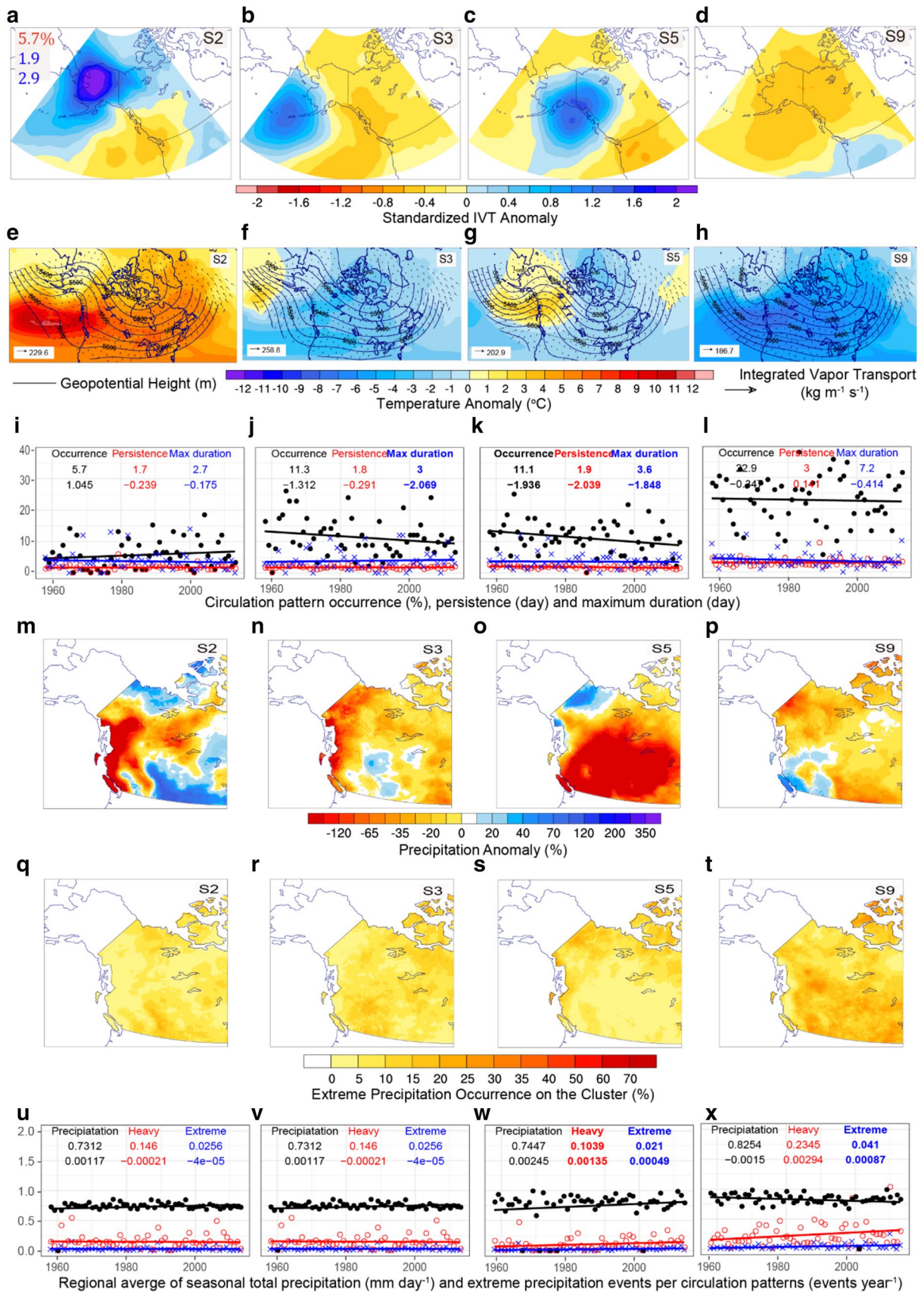
◄**Fig. 4** Same as Fig. 3, but for *spring over Canada West*. The area-weighted mean daily precipitation and occurrences of extreme precipitation events for all spring days over Canada West are 0.756 mm day⁻¹ and 1.8 days (average of 0.201 days for 9 SOM |IVT|′ patterns), respectively

(Fig. S2b). This indicates that pathways for moisture transporting from the North Atlantic to the Arctic have experienced a westward shift, resulting an increase in IVT through the Canada East in spring.

Figure 8 shows matrices of the transition probability within the neighboring days between four |IVT|′ anomaly pattern clusters, while those between nine SOM |IVT|′ anomaly nodes are shown in Fig. S9. Because the persistence of LSMPs is ~ 2 days, a node or a pattern cluster tends to transit to itself with a predominantly high probability (≥ 0.45). Most patterns tend to transit to the dry pattern because of the extremely high occurrence frequency of the dry pattern. However, for Canada East, there has been a higher transition probability of LSMPs in spring between wet patterns (north, south and east pattern clusters) than those in winter (Fig. 8), which also shows the relatively low occurrence frequency of the dry pattern for Canada East in spring (Table S1).

Because patterns within a particular pattern cluster have similar LSMPs (but with different centers of extremely high |IVT|′ anomalies) so that as the synoptic patterns evolved, it was highly likely that a pattern could transit to another node within the same pattern clusters as that pattern for both regions and both seasons. For example, for Canada West, a |IVT|′ pattern at Node S4 (S5) is more likely to transit to Node S5 (S6). The sequential occurrences of Nodes S4–S6 show the movement of the Aleutian Low and a ridge over Canada West propagating with the westerly from the northwest of Canada West and the jet stream extending from Pacific to western North America, respectively (Fig. S5). This sequential pattern transitions also results in the weakening or strengthening of the ridge over northeastern Pacific and western Canada, and the Aleutian Low for Canada West. For Canada East in winter, a frequent transition from Nodes S1 to S3 means a weakening and the Arctic Low shifted in the southeast direction, while the frequent, sequential transition from Nodes S6 to S9 causes the poleward movement of the low-pressure system over Canada East and a shift of the ridge over the North Atlantic in the northeast direction (Fig. S5b). The pattern transitions for Canada East in spring are similar to those in winter, but with less evident movement and less weakening/strengthening of ridges and troughs.

3.4 Precipitation totals and extremes associated with LSMPs

Related to the first and second rows of Figs. 3, 4, 5 and 6, the fourth (fifth) row of Figs. 3, 4, 5 and 6 illustrates how the spatial distributions of winter and spring precipitation anomalies (occurrences of precipitation extremes) over Canada vary with the occurrence of LSMPs. The sixth row of Figs. 3, 4, 5 and 6 shows changes in area-weighted mean seasonal precipitation totals and occurrence of precipitation extremes under each LSMP pattern. As expected, regional positive (negative) seasonal precipitation anomalies across Canada generally occurred in the right (left) of the ridge axis and left (right) of the trough, in the case that the trough points south and the ridge points north (Holton 2004). Different spatial variability of precipitation across Canada among nine nodes results from different center locations and strength of low- and high-pressure systems, and ridges and troughs.

For Canada West in winter, Nodes S7 (S3 and S5) correspond to anomalously wet (dry) condition over the south while dry (wet) condition over the north of Canada West (Fig. 3m-p). The dry (wet) climate over Canada west is associated with Nodes S1–S4 and S7–S8 (S5–S6 and S9). During those days under Nodes S4 and S7–S8, almost the entire Canada West shows negative precipitation anomalies (Fig. S5a). Because the occurrence of dry (wet) nodes for the south of Canada West has increased (decreased), the south of Canada West had become drier. However, the occurrence of dry (wet) nodes for the north of Canada West has decreased (increased), thus resulting in an increase of precipitation over the north of Canada West. More precipitation extremes over the Canadian Prairies are associated with Nodes S6 and S7 (Fig. 3s), while British Columbia with Nodes S6 and S9 (Fig. 3t), and the north of Canada West with Nodes S5 and S9 (Fig. 3r, t). The occurrence of precipitation extremes under Node S6 has significantly decreased, so the occurrence of winter extreme precipitation over the Canadian Prairies has decreased over 1958–2013 (Sect. 3.1). However, both occurrences of Nodes S3–S5 and S9 and their occurrences of precipitation extremes have increased, so there was an increase in occurrences of extreme precipitation over the north of Canada West where the high occurrence frequency of precipitation extremes is associated with Nodes S3–S5 and S9 (Sect. 3.1).

For spring in Canada West, widespread negative (positive) precipitation anomalies over Canada West, i.e., Nodes S3, S5 and S9 (Nodes S4; Fig. S2a), are associated with extremely low (high) |IVT|′ and low (high) surface temperature anomalies over the landmass of Canada West. Nodes showing north–south (Nodes S6 and S8) or east–west (Nodes S2 and S7) contrasting spring precipitation anomalies are associated with the location and direction of a ridge over western North America. Except for Nodes S1–S2 and S6 under which spring precipitation increased, spring precipitation under other six nodes shows a non-significant decrease (Fig. 7). Because both the trends in spring precipitation and spatial variability of spring precipitation anomalies vary
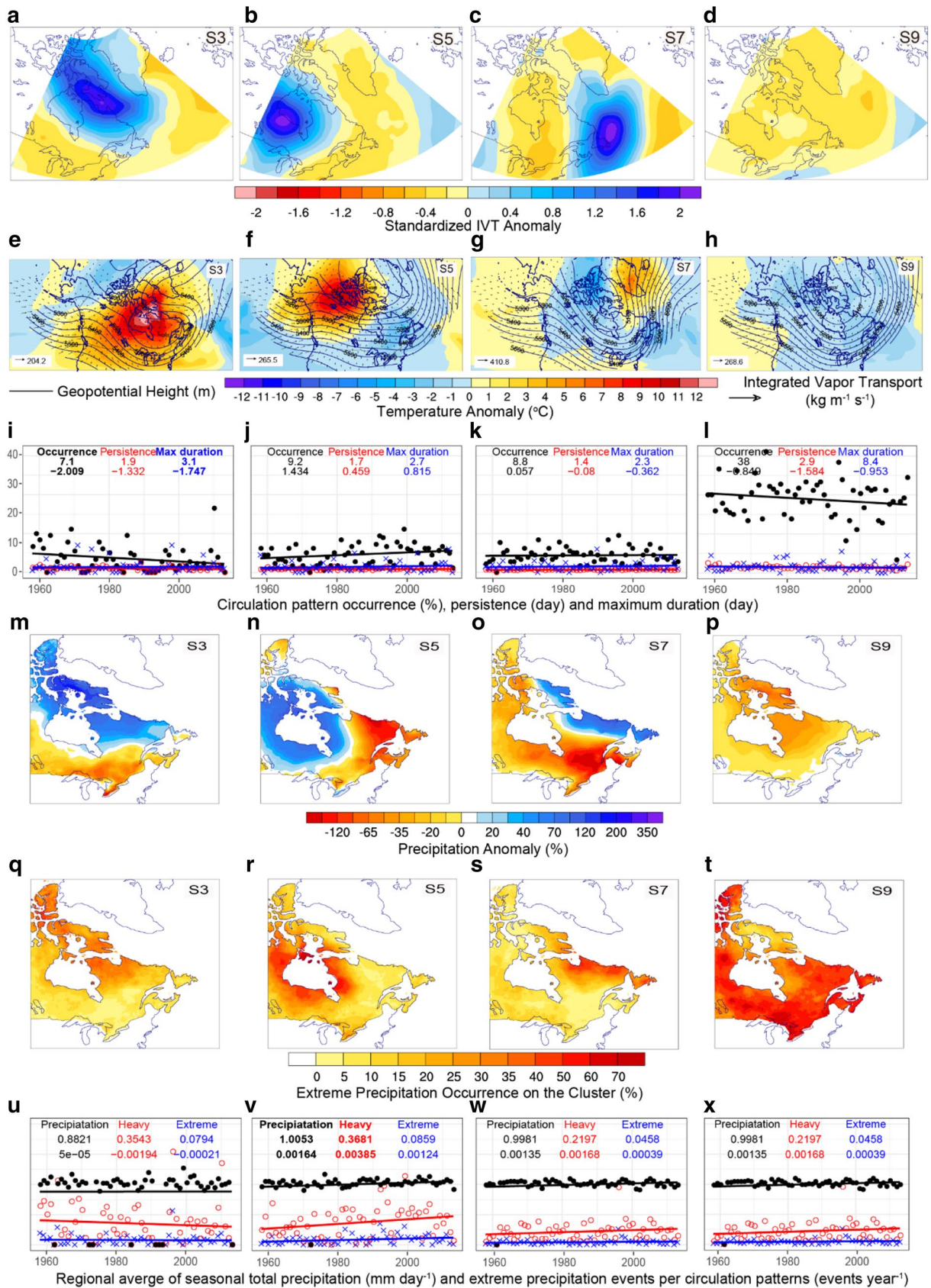
Fig. 5 Same as Fig. 3, but for *winter* over *Canada East*. The area-weighted mean daily precipitation and occurrences of extreme precipitation events for all winter days over Canada East are 0.912 mm day^{-1} and 2.8 days (average of 0.309 days for 9 SOM |IVT|′ patterns), respectively
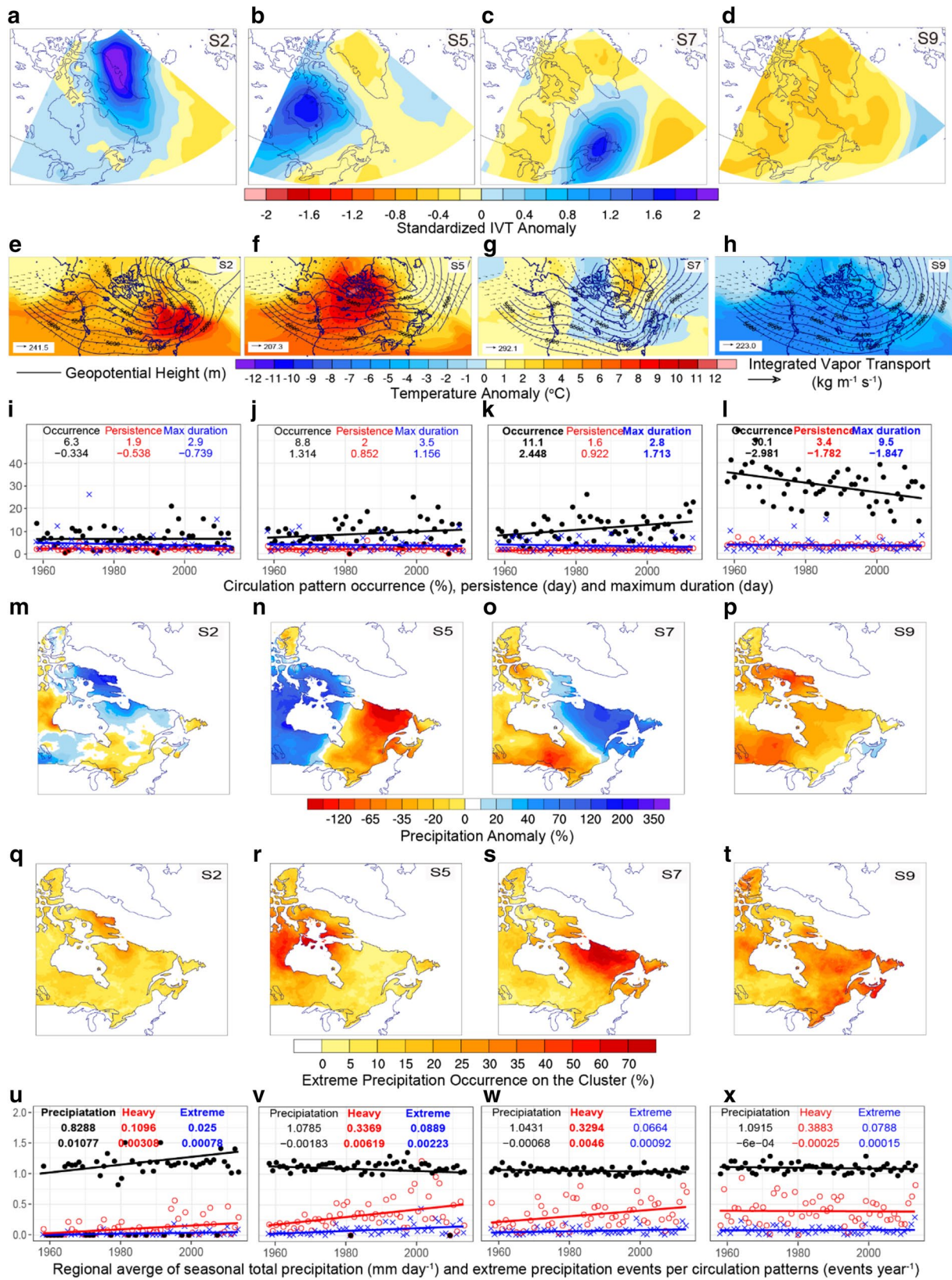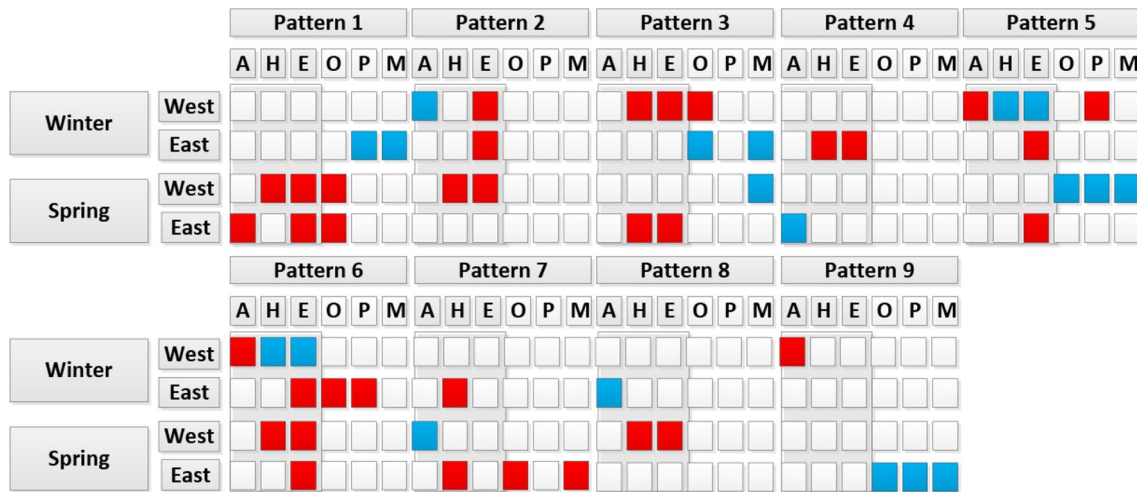
Fig. 6 Same as Fig. 3, but for spring over Canada East. The area-weighted mean daily precipitation and occurrences of extreme precipitation events for all spring days over Canada West are 1.023 mm day^{-1} and 2.4 days (average of 0.261 days for 9 SOM |IVT|′ patterns), respectively

Fig. 7 Trends in land surface precipitation and moisture transport patterns. Trends are calculated for the Canada West and East in winter and spring seasons. Region domains (see Fig. 1) in which a SOM pattern demonstrate statistically significant, increasing (decreasing) trends in the occurrence (O), persistence (P) and maximum duration (M) of standardized integrated vapor transport anomaly (|IVT|′) is shown in red (blue). Regional domains with positive (negative) trends in the average seasonal precipitation (A), occurrence of heavy precipitation (H) and extreme precipitation (E) occurred in each SOM pattern of |IVT|′ is shown in red (blue) which are covered with semi-transparent, grey rectangles. White boxes indicate no statistically significant trends

Fig. 8 One day lead transitional frequencies between the 4 pattern clusters defined in Table S1. The transition probability shows how probable a pattern in a day transits to another pattern (or persist in that pattern) in the following day. For example, the value of 0.19 (0.59) for the Dry pattern of Canada West in winter means that if today's weather is the Dry pattern, then tomorrow's weather would be the North (Dry) pattern with a probability of 19% (59%)

greatly between different nodes, it is difficult to attribute changes in spring precipitation (Sect. 3.1) to changes in the occurrence of LSMPs or the precipitation associated with these LSMPs.

Frequent occurrences of spring extreme precipitation events are associated with both extremely high |IVT|′ and surface temperature anomalies (Nodes S4), and low-pressure blocking systems (Nodes S8 and S9; Fig. S4a), while regions in western British Columbia, Canadian Rockies and the north of Canada West exposed to a ridge shifted eastward also exhibit high occurrence probability of precipitation extremes (Nodes S4 and S6; Fig. S6a). Occurrences of extreme precipitation events under four out of nine LSMPs have significantly increased, and the occurrence of these four patterns has also increased, but only one is statistically significant (Fig. 7). The total increasing magnitude of the

occurrence of extreme precipitation significantly exceeds that of the total decreasing magnitude. This means that occurrences of spring precipitation extremes have increased over Canada West.

For Canada East in winter, extremely low precipitation anomalies are associated with a low-pressure system shifted in the northeast direction (e.g., Nodes S2, S4 and S7–S9; Fig. 5g, h, o, p and S5b) while frequent occurrences of extreme precipitation events are associated with extremely high |IVT|′ anomalies (Nodes S5). As both winter precipitation totals under Nodes S2 and S4–S6 and occurrences of these nodes have increased, the winter precipitation has increased over Canada East. Even though Node S9 shows widespread negative |IVT|′ anomalies, a high percentage of precipitation extremes occurred in days showing similar |IVT|′ patterns as Node S9 (Fig. 5t). This is partly because of its extremely frequent (38%) occurrences and the frequent occurrence of convective precipitation not fully controlled by LSMPs. Although only occurrences of precipitation extremes under Node S5 had significantly increased, the occurrence of precipitation extremes under Nodes S4–S8 associated with frequent precipitation extremes had also increased, but not significant. The increase in occurrences of precipitation extremes under these patterns were concurrent with increasing occurrences of these patterns, thus resulting in more frequent occurrences of winter precipitation extremes over Canada East.

For Canada East in spring, regions with positive (negative) spring precipitation anomalies over Canada East show extremely positive (negative) |IVT|′ anomalies for all patterns (Fig. 6a–d, m–p), while frequent occurrences of spring precipitation extremes are associated with both extremely positive |IVT|′ anomalies (Nodes S5–S7) and uniformly westerly zonal flow (Node S9). Node S1, which shows positive |IVT|′ anomalies for most areas and a trough shifted southeast centered over the landmass of Canada East and a ridge shifted northwest centered over the North Atlantic, are associated with positive spring precipitation anomalies, but precipitation extremes have occurred less frequently. The frequency of precipitation extremes occurring over 7 out of 9 LSMPs has increased, even though the occurrence of corresponding patterns shows both negative and positive trends (Fig. 7). However, the spring precipitation over 6 out of 9 LSMPs has decreased, but most trends are not statistically significant. Because both occurrences of Node S1 and occurrences of precipitation extremes under Node S1 have experienced a significant increase, the occurrence of extreme precipitation has increased.

3.5 Teleconnections

MEI, PDO, PNA, NAO and AO daily indices were classified into nine groups based on the days occurred with each of the

nine patterns. There are significant differences in synoptic type frequency distribution between positive and negative teleconnection conditions for both regions and both seasons (Fig. 9), which demonstrates significant effects of large-scale climate anomalies on occurrences of LSMPs identified by SOM of |IVT|′ anomaly patterns. Additional composite analyses of the teleconnection between the occurrence of LSMPs and the 0-, 1-, 2-, and 3-month lagged climate indices produced similar results as those shown in Fig. 9.

Effects of PNA on occurrences of LSMPs in winter and spring over Canada West are extremely important as occurrences of 8 out of 9 LSMPs significantly correlated with the teleconnection condition of PNA. For Canada West, winter Nodes S3–S5 and S9 (S1–S2 and S6–S7) that are related to hot and dry (cold and wet) climate, and less (more) frequent precipitation extremes over the Canadian Prairies tend to occur during the positive (negative) phase of PNA (Figs. 3, 9). This agrees with low winter precipitation observed over southwestern Canada in winter during negative PNA years (Gan et al. 2007). Spring Nodes S2–S3 (S1 and S4–S6) that are associated with low (high) spring precipitation, low (high) occurrence probability of precipitation extremes, and extremely low (high) |IVT|′ over northern landmass of Canada West, are also more likely to occur during the negative (positive) phase of PNA (Figs. 4, 9). Effects of PNA on occurrences of LSMPs for Canada East are generally not significant.

The effects of AO and NAO on the occurrence of various LSMPs are significant in both winter and spring, especially for Canada East. Since AO and NAO are highly positively correlated, differences between the occurrence frequency of LSMPs between positive and negative AO and NAO are similar to each other. For Canada East in both winter and spring, Nodes S1–S4 which correspond to a hot and dry climate, and less frequent precipitation extremes over the south of Canada East have mostly occurred during the negative phase of NAO while Nodes S6–S9 which are associated with a cold and more frequent extreme precipitation events over the north of Canada East are associated with the positive phase of NAO.

ENSO is found to be significantly associated with occurrences of LSMPs for Canada West that is significantly correlated with MEI, and there were some significant differences in the occurrence frequency of LSMPs between positive and negative MEI for Canada East in winter. Winter Nodes S2–S4 and S7–S9, and spring Nodes S3, S5–S6 and S9 for Canada West correspond to a dry climate and a low occurrence frequency of extreme precipitation events over the south of Canada West tend to occur in years of positive ENSO (El Niño) condition. This is consistent with the results found in other studies (e.g., Bonsal et al. 2001; Gan et al. 2007; Tan and Gan 2017; Tan et al. 2016). However, for Canada East, LSMPs that tend to occur in negative
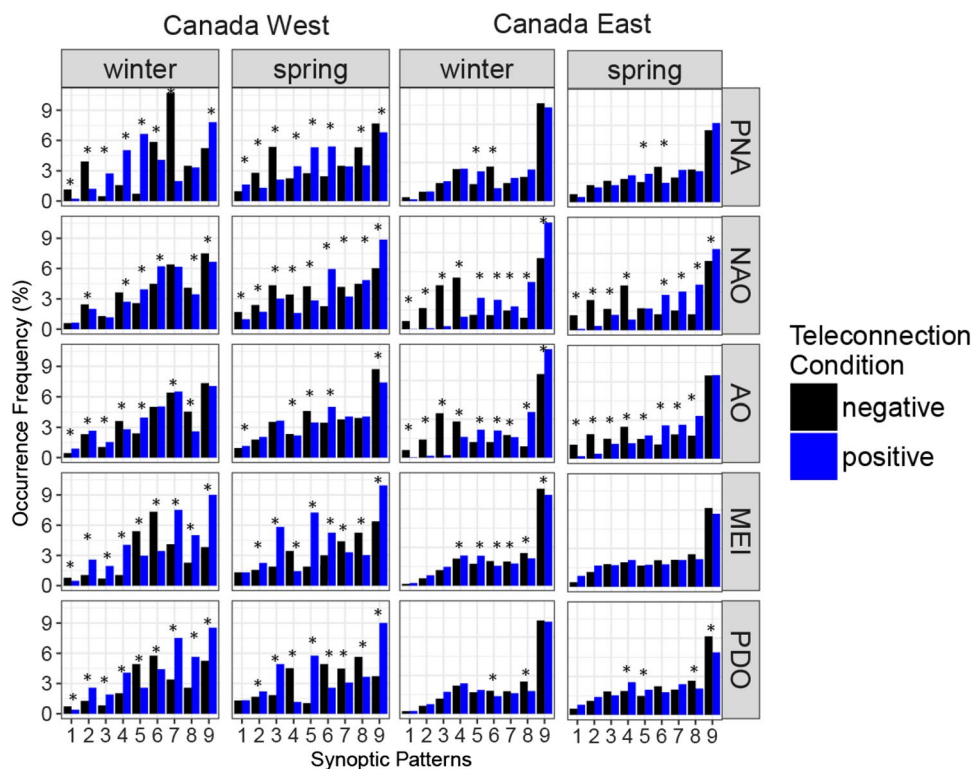
ENSO years (Node S6–S9) are associated with both wet
(Nodes S6–S7) and dry (Nodes S8–S9) climate, which indi-
cates a weak correlation between ENSO and precipitation
in Canada East. Differences in the occurrence frequency
between positive and negative phases of PDO are similar to
those of ENSO regarding the synoptic types of nine LSMPs,
as positive PDO also corresponds to a dry climate and low
occurrence frequency of extreme precipitation.

4 Summary and conclusions

This study identified dominant synoptic moisture pathway
patterns using the SOM algorithm on |IVT|′ over Canada
West and East in winter and spring. Composite mean val-
ues of IVT fields, GPH, and surface temperature for each
SOM |IVT|′ pattern were calculated to obtain LSMPs that
can comprehensively describe synoptic moisture pathways.
Moisture pathways and LSMPs were linked to seasonal pre-
cipitation totals and widespread occurrences of precipitation
extremes. We evaluated changes in characteristics of LSMPs
including frequency, persistence and maximum duration.
One-day lag transitions between different LSMPs were also
estimated. Changes in seasonal precipitation totals and the
occurrence frequency of precipitation extremes under each
LSMP were also identified. Thus, observed changes in sea-
sonal precipitation totals and occurrences of precipitation
extremes were attributed to both the occurrence of LSMPs

and the precipitation under those LSMPs. To study the
effects of large-scale climate anomalies on the occurrence
of LSMPs, composite teleconnection condition of selected
climate indices for each LSMP were also analyzed. The find-
ings of the study are summarized as follows:

1. Synoptic moisture pathways and LSMPs for seasonal
   precipitation totals and occurrences of extreme precipi-
   tation events that had impacted Canada West and East
   in winter and spring were featured by various regions
   exposed to anomalously high IVT, deepened high and
   low pressures, and strengthened troughs and ridges. The
   identified circulation patterns exhibit the propagation of
   jet streams resulted from the Rossby wave resonance, as
   the location and direction of ridges and troughs, and the
   strength and center of pressure lows and highs varied
   considerably. Compared to spring, winter shows a wav-
   ier and more amplified jet stream capable of producing
   extreme precipitation (Mann et al. 2017).

2. Regions showing positive (negative) precipitation
   anomalies for each LSMP are generally located to
   the right (left) of the ridge axis and left (right) of the
   trough which favorably lead to moisture convergence
   (divergence). Even though LSMPs resulting in positive
   precipitation anomalies are associated with more fre-
   quent occurrences of extreme precipitation events than
   those resulting in negative precipitation anomalies, the
   dry patterns featured with anomalously low |IVT|′ are

sometimes associated with more frequent occurrences of extreme precipitation events. Further studies should be conducted to examine whether high frequency of precipitation extremes occurred under dry patterns is caused by the high occurrence frequency of dry patterns or/and particular physical processes that are not associated with LSMPs (e.g., local convective precipitation).

3. Only 17.6% of the annual occurrence characteristics of LSMPs identified show statistically significant changes for winter and spring. There was a significant decrease in occurrences of moist synoptic patterns that are favorable to positive precipitation anomaly and more precipitation extremes in winter over Canada West. The seasonal precipitation and occurrence of precipitation extremes under most moist synoptic patterns had also decreased. Therefore, the seasonal precipitation and the occurrence of extreme precipitation events had dramatically decreased over Canada West in winter.

4. LSMPs resulting in a hot and dry (cold and wet) climate and less (more) frequent extreme precipitation events over the Canadian Prairies in winter and northwestern Canada in spring are more likely to occur in years with the negative (positive) phase of PNA. LSMPs resulting in a wet climate and frequent occurrences of extreme precipitation events over southeastern Canada are associated with the positive phase of NAO. In El Niño years and negative PDO years, occurrences of LSMPs tend to associate with a dry climate and less frequent precipitation extremes over western Canada.

References

Alexander MA, Scott JD, Swales D, Hughes M, Mahoney K, Smith CA (2015) Moisture pathways into the U.S. intermountain west associated with heavy winter precipitation events. J Hydrometeorol 16:1184–1206

Barnett TP, Adam JC, Lettenmaier DP (2005) Potential impacts of a warming climate on water availability in snow-dominated regions. Nature 438:303–309

Barry R, Gan TY, 2011, Global cryosphere, past, present and future. Cambridge University Press, Cambridge ISBN: 9780521769815

Benyahya L, Gachon P, St-Hilaire A, Laprise R (2014) Frequency analysis of seasonal extreme precipitation in southern Quebec (Canada): an evaluation of regional climate model simulation with respect to two gridded datasets. Hydrol Res 45:115–133

Bintanja R, Andry O (2017) Towards a rain-dominated Arctic. Nat Clim Change 7:263–267

Bintanja R, Selten FM (2014) Future increases in Arctic precipitation linked to local evaporation and sea-ice retreat. Nature 509:479–482

Bonsal BR, Shabbar A, Higuchi K (2001) Impacts of low frequency variability modes on Canadian winter temperature. Int J Climatol 21:95–108

Brimelow JC, Reuter GW (2005) Transport of atmospheric moisture during three extreme rainfall events over the Mackenzie River Basin. J Hydrometeorol 6:423–440

Cannon AJ, Sobie SR, Murdock TQ (2015) Bias correction of GCM precipitation by quantile mapping: How well do methods preserve changes in quantiles and extremes? J Clim 28:6938–6959

Cassano EN, Glisan JM, Cassano JJ, Gutowski WJ, Seefeldt MW (2015) Self-organizing map analysis of widespread temperature extremes in Alaska and Canada. Clim Res 62:199–218

Cassano EN, Cassano JJ, Seefeldt MW, Gutowski WJ, Glisan JM (2016) Synoptic conditions during summertime temperature extremes in Alaska. Int J Climatol. https://doi.org/10.1002/joc.4949

Cohen JL, Furtado JC, Barlow MA, Alexeev VA, Cherry JE (2012) Arctic warming, increasing snow cover and widespread boreal winter cooling. Environ Res Lett 7:014007. https://doi.org/10.1088/1748-9326/7/1/014007

Collins M et al (2018) Challenges and opportunities for improved understanding of regional climate dynamics. Nat Clim Change 8:101–108

Coulibaly P (2006) Spatial and temporal variability of Canadian seasonal precipitation (1900–2000). Adv Water Resour 29:1846–1865

Déry SJ, Hernández-Henríquez MA, Burford JE, Wood EF (2009) Observational evidence of an intensifying hydrological cycle in northern Canada. Geophys Res Lett. https://doi.org/10.1029/2009gl038852

Dettinger M (2011) Climate change, atmospheric rivers, and floods in California—a multimodel analysis of storm frequency and magnitude changes. J Am Water Resour As 47:514–523

Dufour A, Zolina O, Gulev SK (2016) Atmospheric moisture transport to the Arctic: assessment of reanalyses and analysis of transport components. J Clim 29:5061–5081

Gan TY (2000) Reducing vulnerability of water resources of Canadian Prairies to potential droughts and possible climatic warming. Water Resour Manag 14(2):111–135. https://doi.org/10.1023/A:1008195827031

Gan TY, Gobena AK, Wang Q (2007) Precipitation of southwestern Canada: wavelet, scaling, multifractal analysis, and teleconnection to climate anomalies. J Geophys Res 112:D10110. https://doi.org/10.1029/2006jd007157

Gibson PB, Perkins-Kirkpatrick SE, Uotila P, Pepler AS, Alexander LV (2017) On the use of self-organizing maps for studying climate extremes. J Geophys Res Atmos 122:3891–3903

Gilaberte-Búrdalo M, López-Martín F, Pino-Otín MR, López-Moreno JI (2014) Impacts of climate change on ski industry. Environ Sci Policy 44:51–61

Gizaw MS, Gan TY (2016) Possible impact of climate change on future extreme precipitation of the Oldman, Bow and Red Deer River Basins of Alberta. Int J Climatol 36:208–224

Harada Y et al (2016) The JRA-55 reanalysis: representation of atmospheric circulation and climate variability. J Meteorol Soc Jpn Ser II 94:269–302

Holton JR (2004) an introduction to dynamic meteorology, 4th eds. Elsevier Academic Press, Amsterdam

Hopkinson RF, McKenney DW, Milewska EJ, Hutchinson MF, Papadopol P, Vincent LA (2011) Impact of aligning climatological day on gridding daily maximum–minimum temperature and precipitation over Canada. J Appl Meteorol Clim 50:1654–1665

Horton DE, Johnson NC, Singh D, Swain DL, Rajaratnam B, Diffenbaugh NS (2015) Contribution of changes in atmospheric circulation patterns to extreme temperature trends. Nature 522:465–469

Hu C et al (2016) Shifting El Nino inhibits summer Arctic warming and Arctic sea-ice melting over the Canada Basin. Nat Commun 7:11721. https://doi.org/10.1038/ncomms11721

Hutchinson MF, McKenney DW, Lawrence K, Pedlar JH, Hopkinson RF, Milewska E, Papadopol P (2009) Development and testing of Canada-wide interpolated spatial models of daily minimum–maximum temperature and precipitation for 1961–2003. J Appl Meteorol Clim 48:725–741

IPCC (2013) The physical science basis. Contribution of working group I to the fifth assessment report of the intergovernmental panel on climate change. In: Stocker TF, Qin D, Plattner G-K, Tignor M, Allen SK, Boschung J, Nauels A, Xia Y, Bex V, Midgley PM (eds.) Climate change 2013. Cambridge University Press, Cambridge

Kendall MG (1975) Rank correlation methods. Charless Griffin, London

Kobayashi S et al (2015) The JRA-55 reanalysis: General specifications and basic characteristics. J Meteorol Soc Jpn Ser II 93:5–48

Kochtubajda B, Mooney C, Stewart R (2017) Characteristics, atmospheric drivers and occurrence patterns of freezing precipitation and ice pellets over the Prairie Provinces and Arctic Territories of Canada: 1964–2005. Atmos Res 191:115–127

Kohonen T (1998) The self-organizing map. Neurocomputing 21:1–6

Lackmann GM, Gyakum JR (1996) The synoptic- and planetary-scale signatures of precipitating systems over the Mackenzie River Basin. Atmos Ocean 34:647–674

Lennard C, Hegerl G (2015) Relating changes in synoptic circulation to the surface rainfall response using self-organising maps. Clim Dyn 44:861–879

Liu C, Barnes EA (2015) Extreme moisture transport into the Arctic linked to Rossby wave breaking. J Geophys Res Atmos 120:3774–3788

Liu J, Stewart RE (2003) Water vapor fluxes over the Saskatchewan River Basin. J Hydrometeorol 4:944–959

Liu J, Stewart RE, Szeto KK (2004) Moisture transport and other hydrometeorological features associated with the severe 2000/01 drought over the western and central Canadian Prairies. J Clim 17:305–319

Loikith PC et al (2015) Evaluation of large-scale meteorological patterns associated with temperature extremes in the NARCCAP regional climate model simulations. Clim Dyn 45:3257–3274

Mann ME, Rahmstorf S, Kornhuber K, Steinman BA, Miller SK, Coumou D (2017) Influence of anthropogenic climate change on planetary wave resonance and extreme weather events. Sci Rep 7:45242. https://doi.org/10.1038/srep45242

Mattingly KS, Ramseyer CA, Rosen JJ, Mote TL, Muthyala R (2016) Increasing water vapor transport to the Greenland ice sheet revealed using self-organizing maps. Geophys Res Lett 43:9250–9258

Mekis É, Vincent LA (2011) An overview of the second generation adjusted daily precipitation dataset for trend analysis in Canada. Atmos Ocean 49:163–177

Mieruch S, Noël S, Bovensmann H, Burrows JP, Freund JA (2010) Markov chain analysis of regional climates. Nonlinear Proc Geophys 17:651–661

Milrad SM, Atallah EH, Gyakum JR (2009a) Dynamical and precipitation structures of poleward-moving tropical cyclones in Eastern Canada, 1979–2005. Mon Weather Rev 137:836–851

Milrad SM, Atallah EH, Gyakum JR (2009b) Synoptic-scale characteristics and precursors of cool-season precipitation events at St. John's, Newfoundland, 1979–2005. Weather Forecast 24:667–689

Milrad SM, Atallah EH, Gyakum JR (2010) Synoptic typing of extreme cool-season precipitation events at St. John's, Newfoundland, 1979–2005. Weather Forecast 25:562–586

Milrad SM, Atallah EH, Gyakum JR, Dookhie G (2014) Synoptic typing and precursors of heavy warm-season precipitation events at Montreal, Québec. Weather Forecast 29:419–444

Najafi MR, Zwiers FW, Gillett NP (2015) Attribution of Arctic temperature change to greenhouse-gas and aerosol influences. Nat Clim Change 5:246–249

Newton BW, Prowse TD, Bonsal BR (2014) Evaluating the distribution of water resources in western Canada using synoptic climatology and selected teleconnections. Part 1: winter season. Hydrol Process 28:4219–4234

Radić V, Cannon AJ, Menounos B, Gi N (2015) Future changes in autumn atmospheric river events in British Columbia, Canada, as projected by CMIP5 global climate models. J Geophys Res Atmos 120:9279–9302

Reusch DB, Alley RB, Hewitson BC (2005) Relative performance of self-organizing maps and principal component analysis in pattern extraction from synthetic climatological data. Polar Geogr 29:188–212

Roberge A, Gyakum JR, Atallah EH (2009) Analysis of intense poleward water vapor transports into high latitudes of western North America. Weather Forecast 24:1732–1747

Rutz JJ, Steenburgh WJ, Ralph FM (2015) The inland penetration of atmospheric rivers over western North America: A lagrangian analysis. Mon Weather Rev 143:1924–1944

Schindler DW, Donahue WF (2006) An impending water crisis in Canada's western prairie provinces. Proc Natl Acad Sci USA 103:7210–7216

Screen JA, Simmonds I (2010) The central role of diminishing sea ice in recent Arctic temperature amplification. Nature 464:1334–1337

Sen PK (1968) Estimates of the regression coefficient based on Kendall's tau. J Am Stat Assoc 63:1379–1389

Sheridan SC, Lee CC (2011) The self-organizing map in synoptic climatological research. Prog Phys Geog 35:109–119

Skific N, Francis JA, Cassano JJ (2009) Attribution of projected changes in atmospheric moisture transport in the Arctic: a self-organizing map perspective. J Clim 22:4135–4153

Smirnov VV, Moore GWK (1999) Spatial and temporal structure of atmospheric water vapor transport in the Mackenzie River Basin. J Clim 12:681–696

Smirnov VV, Moore GWK (2001) Short-term and seasonal variability of the atmospheric water vapor transport through the Mackenzie River Basin. J Hydrometeor 2:441–452

Spence C, Rausch J (2005) Autumn synoptic conditions and rainfall in the subarctic Canadian Shield of the Northwest Territories, Canada. Int J Climatol 25:1493–1506

Spry CM, Kohfeld KE, Allen DM, Dunkley D, Lertzman K (2014) Characterizing pineapple express storms in the lower mainland of British Columbia, Canada. Can Water Resour J 39:302–323

Swales D, Alexander M, Hughes M (2016) Examining moisture pathways and extreme precipitation in the U.S. Intermountain West using self organizing maps. Geophys Res Lett 43:1727–1735

Tan X, Gan TY (2017) Non-stationary analysis of the frequency and intensity of heavy precipitation over Canada and their relations to large-scale climate patterns. Clim Dyn 48:2983–3001

Tan X, Gan TY, Shao D (2016) Wavelet analysis of precipitation extremes over Canadian ecoregions and teleconnections to large-scale climate anomalies. J Geophys Res Atmos 121:14469–14486

Tan X, Gan TY, Chen YD (2018a) Moisture sources and pathways associated with the spatial variability of seasonal extreme precipitation over Canada. Clim Dyn. https://doi.org/10.1007/s00382-017-3630-0

Tan X, Gan TY, Chen YD (2018b) Synoptic moisture pathways associated with mean and extreme precipitation over Canada for summer and fall. Clim Dyn. https://doi.org/10.1007/s00382-018-4300-6

Vavrus SJ, Wang F, Martin JE, Francis JA, Peings Y, Cattiaux J (2017) Changes in North American atmospheric circulation and extreme weather: Influence of Arctic amplification and northern hemisphere snow cover. J Clim. https://doi.org/10.1175/jcli-d-16-762.1

Vihma T et al (2015) The atmospheric role in the Arctic water cycle: a review on processes, past and future changes, and their impacts. J Geophys Res Biogeosci 121:586–620

Vincent LA et al (2015) Observed trends in Canada's climate and influence of low-frequency variability modes. J Clim 28:4545–4560

Walsh JE (2014) Intensified warming of the Arctic: causes and impacts on middle latitudes. Glob Planet Change 117:52–63

Wang XL, Wan H, Swail VR (2006) Observed changes in cyclone activity in Canada and their relationships to major circulation regimes. J Clim 19:896–915

Wang G, Wang D, Trenberth KE, Erfanian A, Yu M, Bosilovich MG, Parr DT (2017) The peak structure and future changes of the relationships between extreme precipitation and temperature. Nat Clim Change 7:268–274

Wehrens R, Buydens LMC (2007) Self- and super-organizing maps in R: the kohonen package. J Stat Softw 21(5). https://doi.org/10.18637/jss.v021.i05

White R, Etkin D (1997) climate change, extreme events and the Canadian insurance industry. Nat Hazards 16:135–163

Wolter K, Timlin MS (2011) El Niño/Southern Oscillation behaviour since 1871 as diagnosed in an extended multivariate ENSO index (MEI.ext). Int J Climatol 31:1074–1087

Zhang X, He J, Zhang J, Polyakov I, Gerdes R, Inoue J, Wu P (2013) Enhanced poleward moisture transport and amplified northern high-latitude wetting trend. Nat Clim Change 3:47–51

Zhang X, Zwiers FW, Li G, Wan H, Cannon AJ (2017) Complexity in estimating past and future extreme short-duration rainfall. Nat Geosci 10:255–259